ACS APPLIED MATERIALS & INTERFACES

Research Article

www.acsami.org

Extremely Sensitive and Selective NO Probe Based on Villi-like WO_3 Nanostructures for Application to Exhaled Breath Analyzers

Hi Gyu Moon,[†,‡] You Rim Choi,[§] Young-Seok Shim,[†,§] Kwon-Il Choi,[∥] Jong-Heun Lee,[∥] Jin-Sang Kim,[†] Seok-Jin Yoon,[†] Hyung-Ho Park,[‡] Chong-Yun Kang,*[,†,⊥] and Ho Won Jang*[,§]

[†]Electronic Materials Research Center, Korea Institute of Science and Technology, Seoul 136-791, Republic of Korea

[‡]Department of Materials Science and Engineering, Yonsei University, Seoul 120-749, Republic of Korea

[§]Department of Materials Science and Engineering, Research Institute of Advanced Materials, Seoul National University, Seoul 151-744, Republic of Korea

[∥]Department of Materials Science and Engineering, Korea University, Seoul 136-713, Republic of Korea

[⊥]IT-NS, KU-KIST School, Korea University, 145, Anam-ro, Seongbok−gu, Seoul 136-701, Republic of Korea

Supporting Information

ABSTRACT: Self-assembled WO_3 thin film nanostructures with 1-dimensional villi-like nanofingers (VLNF) have been synthesized on the SiO_2/Si substrate with Pt interdigitated electrodes using glancing angle deposition (GAD). Room-temperature deposition of WO_3 by GAD resulted in anisotropic nanostructures with large aspect ratio and porosity having a relative surface area, which is about 32 times larger than that of a plain WO_3 film. A WO_3 VLNF sensor shows extremely high response to nitric oxide (NO) at 200 °C in 80% of relative humidity atmosphere, while responses of the sensor to ethanol, acetone, ammonia, and carbon monoxide are negligible. Such high sensitivity and selectivity to NO are attributed to the highly efficient modualtion of potential barriers at narrow necks between individual WO_3 VLNF and the intrinsically high sensitivity of WO_3 to NO. The theoretical detection limit of the sensor for NO is expected to be as low as 88 parts per trillion (ppt). Since NO is an approved biomarker of chronic airway inflammation in asthma, unprecedentedly high response and selectivity, and ppt-level detection limit to NO under highly humid environment demonstrate the great potential of the WO_3 VLNF for use in high performance breath analyzers.

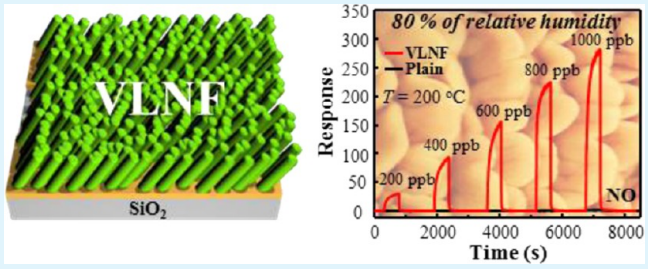

KEYWORDS: *semiconducting metal oxide gas sensor, WO_3 nanostructures, glancing angle deposition, NO probe, exhaled breath analyzer*

INTRODUCTION

Chemoreistive sensors based on semiconducting metal oxides have attracted enormous attention for diverse applications such as environmental monitoring, food processing, semiconductor processing, agriculture, automotive and aerospace industries, and medical diagnosis.[1−7] Among these applications, the detection of human diseases such as lung cancer, asthma and diabetes by analyzing exhaled breath is an emerging field of medical diagnostic, which can be noninvasive and cost-effective alternatives to conventional blood analysis methods.[8−10] In general, human breath is a mixture of nitrogen, carbon dioxide, nitric oxide, ammonia, water vapor, and more than 1000 volatile traces with concentrations ranging from several ppt to several ppm.[11−13] Due to this complexity, the selective detection of a target gas in human breath using metal oxide-based chemoresistive sensors is challenging because metal oxides have large responses to both oxidizing and reducing gases such as NO, NO_2, CO, H_2, NH_3, and volatile organic compounds including ethanol and acetone. For high and rapid response, semiconductor chemoresistive sensors should be operated at elevated temperatures (> 200 °C) in which gas adsorption and desorption on the surface become active.[14]

Detecting a NO concentration higher than 30 parts per billion (ppb) in exhaled breath indicates that the human may suffer from asthma due to inflammatory response in the airways,[15−17] which is especially serious for young children. A high performance chemoresistive sensor for breath analyzers to diagnose asthma necessitates an extremely sensitive and selective NO sensing material, which should have ppb-level detection limits under a highly humid environment (relative humidity (RH) > 80%).[18] In general, NO detection limits of conventional chemoresistive sensors based on SnO_2 nanoparticles under dry ambience are around 1 ppm or higher.[19] To achieve lower detection limits, chemoresistive sensors based on 1-dimensional (1D) metal oxide materials including nanowires, nanorods, nanotubes, and nanobelts have been widely exploited

Received: June 25, 2013
Accepted: October 4, 2013
Published: October 4, 2013

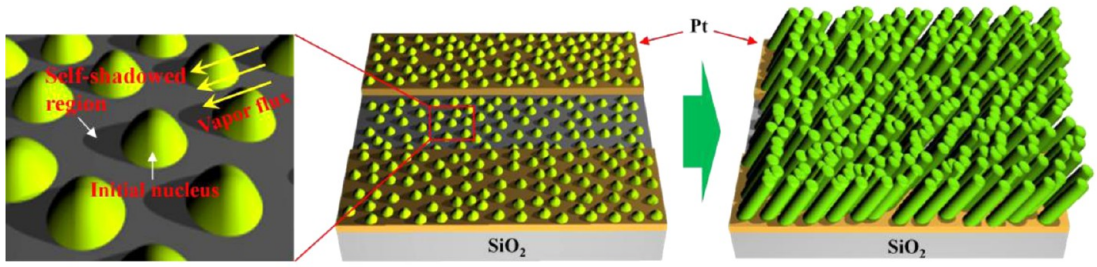

Figure 1. Schematic diagram of the synthesis of a porous VLNF WO_3 thin film on a SiO_2/Si substrate with Pt IDEs using GAD.

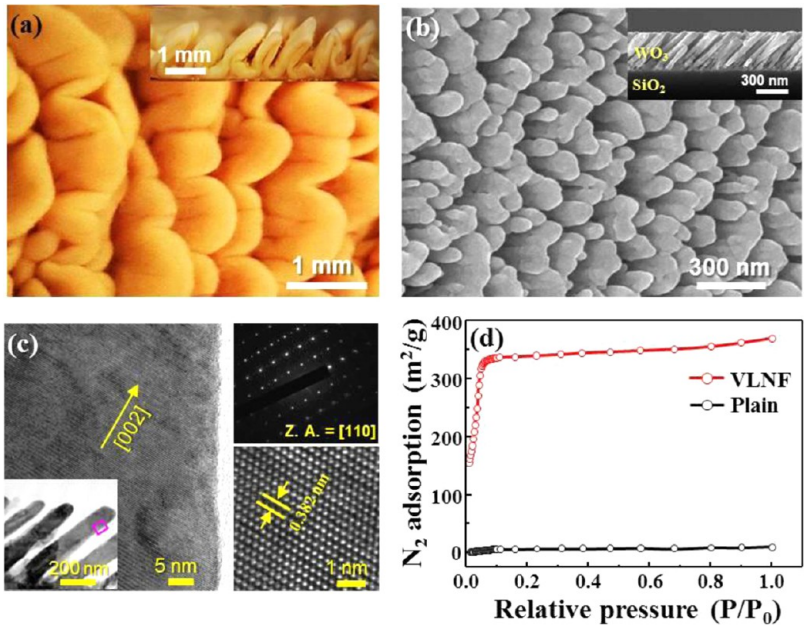

Figure 2. (a) Plain-view and cross-sectional (inset) photographs of chicken intestine villi. (b) Plain-view and cross-sectional (inset) scanning electron microscopy (SEM) images of a WO_3 thin film with 1D VLNF. (c) High resolution TEM image with a selected area diffraction pattern and a lattice image. The area of the high-resolution image is highlighted in the inset. (d) N_2 adsorption isotherms of a 380 nm thick WO_3 film with VLNF and a 380 nm thick plain WO_3 film at 200 °C.

recently.[20−22] Rout et al.[23] and Li et al.[24] demonstrated the ppb-level detection of NO using In_2O_3, WO_3 nanowires and reduced graphene oxide (rGO) , respectively. However, the use of 1D nanomaterials and rGO as chemoresistive sensors is still in the beginning stage in how to integrate them with low-cost and high-yield mass production process. As an alternative, porous thin films based on 1D metal oxide nanostructures are considered as more desirable configuration for chemoresistive sensors due to their simplicity in synthesis, high reproducibility, and excellent compatibility to the well-established semiconductor fabrication processes.[25] Although highly sensitive detection of various gases using porous thin film sensors based on ZnO,[26,27] SnO_2,[28] TiO_2,[29] and WO_3[30] 1D nanostructures has been reported, as far as we know, the selective detection of ppb-level NO using porous thin films based on metal oxide 1D nanostructures has not been studied yet, in particular under a highly humid environment similar to exhaled breath.

In this study, we report facile synthesis and superior chemoresistive properties of porous thin films based on WO_3 1D nanostructure with villi-like nanofinger (VLNF) structures and high surface to volume ratios. The porous WO_3 thin films show remarkably sensitive and selective sensing properties to NO and NO_2 (oxidized state of NO in air atmosphere) at 150−250 °C in 80% of RH. Especially, the theoretical detection limit of NO in a thin film sensor based on the WO_3 1D nanostructure is as low as 88 ppt, which is far below the NO concentration (> 30 ppb) in exhaled breath of patients with asthma.[11] In addition, the response to NO is more than 150 times higher than those to ethanol, acetone, NH_3, and CO at 200 °C in 80% of RH atmosphere

EXPERIMENTAL SECTION

The fabrication process of the porous VLNF WO_3 thin films, which were deposited onto the SiO_2/Si substrate with Pt interdigitated electrodes (IDEs) by glancing angle deposition (GAD)[31] via rf sputtering, is shown in Figure 1. Pt (150 nm thick) IDE patterns of 5 μm spacing were fabricated on a SiO_2/Si substrate using photolithography and dry etching. After patterning the Pt IDEs, a 380 nm WO_3 thin film was deposited onto pre-specified regions (1 mm ×1 mm) by a shadow mask on the Pt IDEs patterned SiO_2/Si substrate using rf sputtering at room temperature. A polycrystalline WO_3 target with 2 inch was utilized for the film deposition. To make the porous film, the sputtering deposition was carried out at a glancing angle (5°). The base pressure, working pressure, RF power, and gas flow rate were 2×10^{-6} mTorr, 3 mTorr, 350 W, and 30 sccm, respectively. The deposition rate of the film was 9.2 nm/min. At this point, the size of the initial nuclei and the deposition rate appear to be key parameters in determining the highly porous nanostructure. The fabricated porous WO_3/Pt/SiO_2 sensor was annealed in air at 500 °C for 60 min to crystallize the porous WO_3 film. For comparison with the porous film,

a sensor based on dense WO_3 thin film (380 nm thick) was fabricated using on-axis RF sputtering.

Morphologies of the fabricated sensors were characterized by FE-SEM (SU-70, Hitachi) using 15 kV. TEM images were taken by a JEOL JEM 2100F with a probe-Cs corrector. A cross-sectional TEM specimen of a WO_3 thin film with villi-like nanostructure on a SiO_2/Si substrate was prepared by mechanical polishing and ion milling with Ar ions. The crystallinity and phase of the WO_3 films were characterized by glancing angle X-ray diffraction (D/Max-2500, Rigaku), where Cu Kα radiation (wavelength = 1.5418 Å) was used for the X-ray source and the incident angle was fixed at a small angle (2°). For the TEM and the X-ray analysis, a WO_3 thin film with villi-like nanostructure was grown on the large area of SiO_2/ Si substrates by the same deposition procedure for the sensor fabrication. The diffraction peaks could be indexed with a pure monoclinic phase of WO_3 with lattice constants a = 7.327 Å, b = 7.564 Å, c = 7.727 Å, and β = 90.488° (JCPDS Card No. 89-4476). The Brunauer–Emmett–Teller (BET) surface area of the films was measured by nitrogen adsorption at 200 °C using a surface area analyzer (QUADRASORB SI, Quantachrome Instruments).

The gas sensing properties of the fabricated WO_3 thin film sensors were measured using external heating by a box furnace. As the flow gas was changed from ambient (nitrogen for NO and dry air for other gases) to a calibrated test gas (balanced with nitrogen for NO and dry air for other gases, Sinyang Gases) in 80% of relative humidity atmosphere, the variation of the sensor resistance was monitored using a source measurement unit (Keithley 236). A constant flow rate of 500 sccm was used during the change of atmosphere from ambient to test gas. The sensor resistance was measured under a DC bias voltage of 1 V. The response of the sensors ($R_{gas}/R_{ambient}$ for NO and NO_2, or $R_{ambient}/R_{gas}$ for ethanol, acetone, NH_3, and CO) was determined by measuring the baseline resistances of the sensors in ambient atmosphere and the fully saturated resistances after exposure to the test gas in 80% of RH atmosphere. Gas flow was controlled using mass flow controllers (MFC), and all measurements were recorded to a computer through the use of LabVIEW over the GPIB interface.

RESULTS AND DISCUSSION

Our key idea to obtain porous metal oxide thin films with large specific surface area is mimicking intestinal villi. Villi are finger-like protrusions covering the inner surface of small intestines of mammals, greatly increasing the surface area for the effective digestion of foods. Figure 2a shows optical images of chicken intestinal villi. By glancing angle deposition (GAD) using an rf sputter, we could achieve porous WO_3 thin film nanostructures that look similar to the chicken intestinal villi, as shown in Figure 2b. Due to the self-shadowing effect, as illustrated in Figure 1, the as-deposited films by GAD are porous with 1D villi-like nanofingers (VLNF). With increasing the film thickness, length to diameter aspect ratios of individual VLNF increases, while the porosity of the films decreases, as summarized in Table 1 (see Figure S1 in the Supporting Information). According to the Table 1 and Figure S2 in the Supporting Information, we could get maximum gas response from the 380-nm-thick film, in which the porosity was about 37% and the diameters of VLNF were 40–50 nm. Therefore, we could directly deposit the porous 380-nm-thick WO_3 film on SiO_2/Si substrates with Pt IDEs of 5 μm spacing (see Figure S3 in the Supporting Information). We could use the films as chemoresistive sensors. For structural characterizations and gas sensing measurements, all the films were annealing at 500 °C for crystallization.

Table 1. Porosity and Length to Diameter Aspect Ratio of the Porous VLNF WO_3 Thin Films as a Function of Film Thickness

thickness of film (nm)	porosity (%)	aspect ratio
70	21	1.5
160	42	4.6
380	37	9.7
540	35	13.2
740	32	15.9
860	31	17.1

Brunauer–Emmett–Teller (BET) measurements revealed that the BET surface area of the WO_3 film with VLNF (~350 m^2/g) is about 32 times larger than that of a plain (dense) WO_3 film (~16 m^2/g), as shown in Figure 2d. For each film, the measured value is not absolute due to contributions from the substrate. Nonetheless, this result shows clearly that the VLNF WO_3 thin films exhibit much larger surface areas than the reference plain film.

To characterize the structure of the porous VLNF WO_3 thin film, the high-resolution transmission electron microscopy (TEM) and the selected area electron diffraction (SAED) patterns are shown in Figure 2c with the inset image which highlighted by a pink rectangle displaying a low-magnification TEM image of the nanocolumn along the [002] growth direction. Even though the WO_3 film with VLNF is polycrystalline as indicated by X-ray diffraction (see Figure S4 in the Supporting Information), the high-resolution transmission electron microscopy (TEM) images show that individual VNLF are near single crystalline with smooth surface.

Figure 3a show responses of a chemoresistive sensor based on the 380-nm-thick WO_3 film with VLNF (VLNF sensor) to 1 ppm NO, NO_2 and 5 ppm ethanol as a function of operating temperature in 80% of RH atmosphere. The response, S, is defined as $R_{gas}/R_{ambient}$ for the oxidizing gas NO_x (NO, NO_2) and $R_{ambient}/R_{gas}$ for the reducing gases (ethanol) where R_{gas} and $R_{ambient}$ denote the sensors' resistances in the presence and absence of a test gas, respectively. Highly sensitive and selective NO and NO_2 sensing properties of the VLNF sensor is clearly observed. The responses to 1 ppm NO and NO_2 reach 278 and 300 at 200 °C, respectively. Under a dry atmosphere, the response of VLNF sensor to 1 ppm NO is 450 (see Figure S5 in the Supporting Information), which is dramatically higher and considered to be the highest value compared with the response values of previous reported sensors based on WO_3 nanoparticles (1.6 to 1 ppm NO at 400 °C),[32] metal (Ag, Pd, and Pt) decorated WO_3 nanoparticles (less than 5 to 2 ppm NO at 220 °C)[33] and WO_3 nanowires (10 to 1 ppm NO at 250 °C).[23] When the temperature increases over 250 °C, the response to NO_x decreases, while the responses to ethanol slightly increase. This indicates that the optimum temperature for the detection of NO_x is 200 °C, which is consistent with previous studies on chemoresistive NO and NO_2 sensors.[34] The fact that the responses change according to the operating temperature show the amount of chemisorbed oxygen play an important role in the mechanism of NO and NO_2 detection. Generally, the operating temperature affects the kinetics of the adsorption on the active surface and leads to the change of gas response.[35,36] At less than 200 °C, oxygen adsorption and surface reaction are generated by sufficient thermal energy, which is effective to overcome the activation energy barrier. Thus, the response of VLNF sensor increases to 200 °C. However, when the operating temperature increases (> 200 °C), the desorption process on the active surface is dominant.[35] Consequently, the responses tend to decrease as the increases

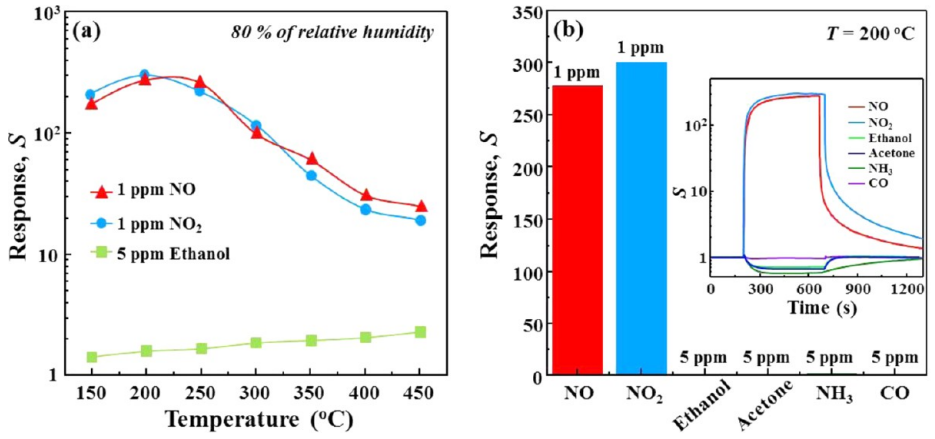

Figure 3. (a) Responses of the VLNF sensor to 1 ppm NO, NO_2 and 5 ppm ethanol in 80% of relative humidity atmosphere as a function of temperature. (b) Response and response curves (inset) of the VLNF sensor to 1 ppm NO_x, 5 ppm ethanol, acetone, NH_3, and CO at 200 °C in 80% of RH atmosphere.

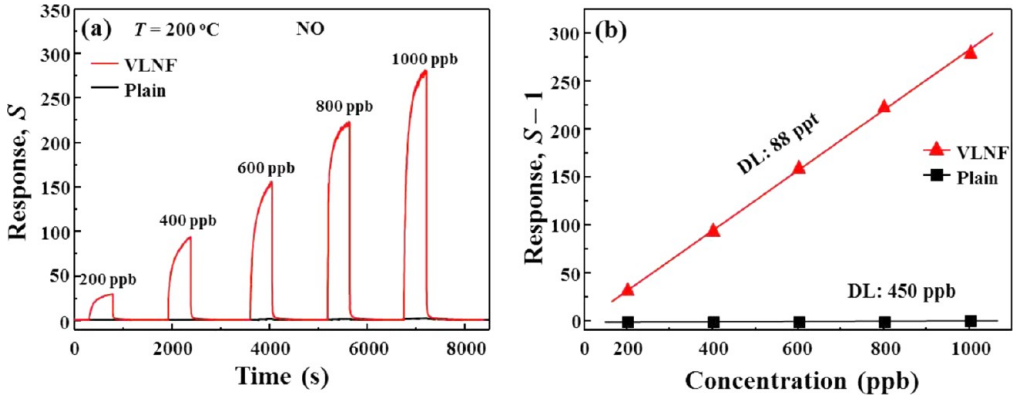

Figure 4. (a) Dynamic sensing transients of the VLNF sensor and a sensor based on a dense plain WO_3 film (plain sensor) to 0.2−1 ppm NO at 200 °C in 80% of relative humidity atmosphere. (b) Response of the VLNF and plain sensors as a function of NO concentration at 200 °C. Theoretical detection limits (DL) of both sensors are presented.

of operating temperature due to the thinner depletion layer at high temperature.[37]

For 5 ppm ethanol, acetone, NH_3, and CO, the VLNF sensor showed responses less than 2 at 200 °C, as shown in Figure 3b and inset. Thus the response ratios, S_{NOx}/S_{gases} are higher than 150 (see Figure S6 in the Supporting Information). Because NO molecules have the better activity than oxygen for adsorption on the oxide surface, NO is not separated easily from the surface in the off state of the gas. In this reason, the recovery to the original baseline resistance by the adsorption of oxygen molecules on the surface is relatively lower than the response. In general, the operating temperature is a critical factor to improve the gas sensing performance of a metal oxide chemoresistive sensor because the amount of ionized oxygen species (O^-, O_2^-, O^{2-}) on the surface of the metal oxide changes with the operating temperature, leading to changes in both sensor resistance and response.[34] For relatively low temperatures, there are much less ionized oxygen species on the surface of the metal oxide. Therefore, reducing gases such as ethanol, acetone, NH_3, and CO have a poor sensitivity at high temperature. On the other hand, oxidizing gases such as NO_x have a high sensitivity at relatively low temperatures ranging from 150−250 °C due to the electron-traped force of the NO_x molecules. An extremely selective NO_x-sensing mechanism at low temperature can be explained as the following. The molecular NO_x has an unpaired electron and is known as a strong oxidizer than other gases.[38] Upon NO_x adsorption, electron transport is likely to occur from nanostructure WO_3 to NO_x because of the electron-traped force of the NO_x molecules at low temperature. Consequently, the vividly high selectivity of the VLNF sensor to NO_x with negligibly low cross-response to ethanol, acetone, NH_3, and CO, which are well-known reactive gases that might be included in human breath with concentrations ranging from several ppb to several ppm demonstrates a strong potential for detecting NO in human breath. A closer look reveals that the maximum responses to ethanol at 450 °C are much lower than the response to NO_x at 200 °C, reflecting that WO_3 itself has a high selectivity to NO_x relative to other metal oxide semiconductors including SnO_2, the most common material for chemoresistive sensors.[34]

A typical response curve of the VLNF sensor to 0.2−1 ppm NO at 200 °C in 80% of RH is shown in Figure 4a. For comparison, the response of a dense plain sensor fabricated by rf-sputtering is also plotted. Upon exposure to oxidizing NO, the VLNF sensor quickly responds with increase in the resistance, which indicates that the WO_3 film is an n-type semiconductor. Compared with the reference sensor based on a dense plain WO_3 film (plain sensor), the VLNF sensor exhibits about 200 times higher responses to 1 ppm NO. Even at an extremely low concentration of 200 ppb, the VLNF sensor shows clear response, which is the first experimental demonstration on detecting ppb-level NO in highly RH

atmosphere using a chemoresisitive sensor in our best knowledge. In addition, for dynamic sensing transients and response to 5 consecutive pulses at NO concentration ranging from 0.2−1 ppm and 5 ppm, the resistances are completely recovered after reacting test gas, as shown in Figure 4a and Figure S7 in the Supporting Information. Therefore, the VLNF is possible for reusable sensor with very stable operation.

In order to estimate the NO detection limit of the VLNF and plain sensors, the response values, $S - 1$, are plotted as a function of NO concentration in a linear scale in Figure 4b. The linear relationship between the response value and the concentration for the VLNF sensor demonstrates the feasibility and the operation capabilities of the sensor for real applications. By applying linear least-square fits to the data, the theoretical detection limit of the VLNF sensor (signal-to-noise ratio > 3)[39] is estimated to be as low as 88 ppt, whereas that of the plain sensor is only 450 ppb. The NO detection limit of the VLNF sensor is much lower than the asthma diagnostic standard levels for NO (30−50 ppb).[40,41]

This result strongly suggests that a main factor for the ultrahigh response of the VLNF sensor is indubitably the porous nanostructure with narrow necks between intergrain boundaries of the WO_3 formed by annealing at 500 °C for 1 h, as shown in Figure 5 a and b with 40°-tilted SEM images of the VLNF WO_3 film between Pt electrodes. In general, semiconductor gas sensor utilizes the change of electrical resistance by gas absorption in potential barrier height between grain boundaries (transducer function), and it is well known that the response increases with decreasing the particle size.[42] It is also noted that previous study by Xu et al. suggested that the response can be controlled by a grain size effect for WO_3 crystallites smaller than 33 nm.[43] Based on these fundamental mechanisms, as shown in Figure 5c with the nano-sized narrow necks of WO_3 (10−30 nm in width), a whole region of the narrow necks are change to the full depletion area (space-charge layer) by NO adsorption. This phenomenon significantly increases the double Schottky barrier heights[44] in the intergrain boundaries of the WO_3 aggregates, which results in a large increase of the conductance for the nanocrystalline material upon exposure to NO.[44] Therefore, we believe that the narrow necks with high chemoresistive variation as well as the gas accessible nanostructures with high surface area play a critical role in the remarkably enhanced sensing properties.[45]

CONCLUSION

We have synthesized porous WO_3 thin films with 1D VLNF using GAD, which were inspired by intestinal villi. Compared with the plain sensor, the VLNF sensor showed ultrahigh response to NO, which is attributed to the large specific surface area and the porous structure with narrow necks. The NO detection limit down to 88 ppt and the extremely high selectivity to NO relative to ethanol, acetone, NH_3 and CO under a highly humid environment suggest that the WO_3 thin film nanostructures mimicking intestinal villi using GAD are very promising for use in high quality sensor elements for breath analyzers to diagnose asthma. We also expect that the porous WO_3 thin film is potentially applicable to the detection of NO in aqueous solution. The additional virtue, the simplicity in the synthesis method, would broaden the applications of the porous VLNF WO_3 thin films to various devices including sensors, water splitting cells, batteries and photochromic glasses.[46−50]

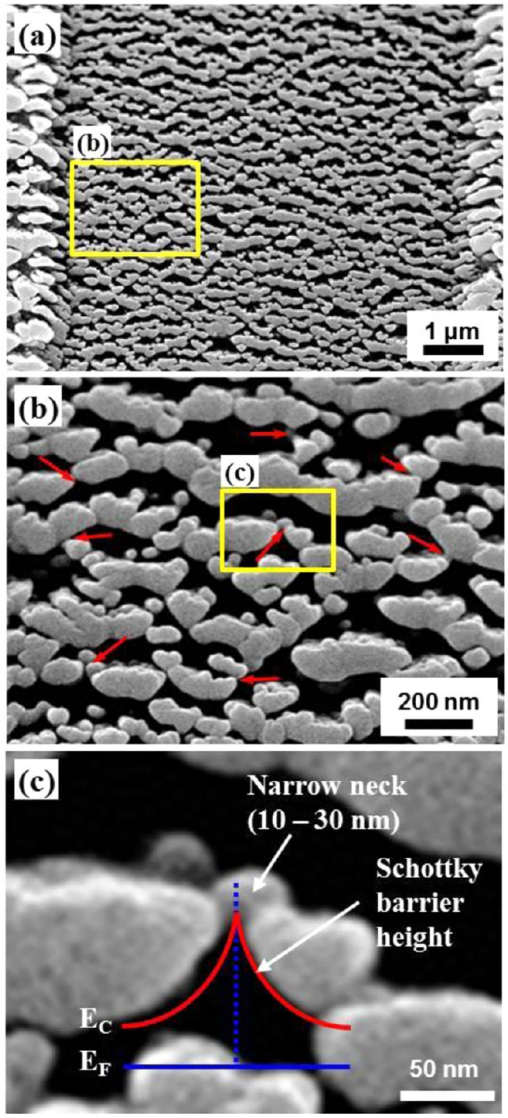

Figure 5. (a) 40°-tilted SEM images of the 380-nm-thick porous WO_3 film between Pt electrodes. (b) The enlarged images highlight the meander of the nanostructures and the presence of narrow necks, indicated with arrows. (c) The magnified images highlight the narrow necks between grain boundaries. At the narrow necks, Schottky barrier heights for electron transfer are enhanced due to the size effect.

ASSOCIATED CONTENT

Supporting Information

The porous VLNF WO_3 thin films with various thickness; gas response to 50 ppm CO for the porous WO_3 thin film nanostructures as a function of film thickness in a dry atmosphere; synthesis of the porous WO_3 thin film on a SiO_2/Si substrate with Pt IDEs; XRD patterns for a 380 nm thick porous VLNF WO_3 thin film; dynamic sensing properties of the VLNF sensor to 1−5 ppm NO in a dry atmosphere at 200 °C; response ratio, S_{NOx}/S_{gas} for the WO_3 VLNF sensor at 200 °C in 80 % of RH atmosphere. This material is available free of charge via the Internet at http://pubs.acs.org.

AUTHOR INFORMATION

Corresponding Authors

*Tel: +82-2-880-1720. Fax: +82-2-884-1413. E-mail: cykang@kist.re.kr.

*E-mail: hwjang@snu.ac.kr.

Notes

The authors declare no competing financial interest.

■ ACKNOWLEDGMENTS

This work was supported by the Korea Ministry of Intelligence and Economy, the Korea Institute of Science and Technology, the Korea Ministry of Environment. H.G.M. acknowledges a Hi Seoul Science Fellowship funded by the Seoul Scholarship Foundation. H.W.J. acknowledges the financial support of the Fusion Research Program for Green Technologies through the National Research Foundation of Korea Grant and the Center for Integrated Smart Sensors funded by the Ministry of Science, ICT & Future Planning as the Global Frontier Project.

■ REFERENCES

(1) Oprea, A.; Courbat, J.; Briand, D.; Barsan, N.; Weimar, U.; De Rooij, N.F. *Sens. Actuators, B* **2012**, *171-172*, 190−197.
(2) Hagleitner, C.; Hierlemann, A.; Lange, D.; Kummer, A.; Kerness, N.; Brand, O.; Baltes, H. *Nature* **2001**, *414*, 293−296.
(3) Romain, A. C.; Nicolas, J. *Sens. Actuators, B* **2010**, *146*, 502−506.
(4) Kolmakov, A.; Moskovits, M. *Annu. Rev. Mater. Res.* **2004**, *34*, 151−180.
(5) Tsai, C.-J.; Chen, M.-L.; Ye, A.-D.; Mao, I.-F. *Sens. Actuators, B* **2012**, *169*, 248−254.
(6) Moos, R.; Muller, R.; Plog, C.; Knezevic, A.; Leye, H.; Irion, E.; Braun, T.; Marquardt, K.-J.; Binder, K. *Sens. Actuators, B* **2002**, *83*, 181−189.
(7) Kolmakov, A.; Zhang, Y.; Cheng, G.; Moskovits, M. *Adv. Mater.* **2003**, *15*, 997−1000.
(8) Peng, G.; Tisch, U.; Adams, O.; Hakim, M.; Shehada, N.; Broza, Y. Y.; Billan, S.; Abdah-Bortnyak, R.; Kuten, A.; Haick, H. *Nat. Nanotechnol.* **2009**, *4*, 669−673.
(9) Smith, A. D.; Cowan, J. O.; Filsell, S.; McLachlan, C.; Monti-Sheehan, G.; Jackson, P.; Robin Taylor, D. *Am. J. Respir. Crit. Care Med.* **2004**, *169*, 473−478.
(10) Righettoni, M.; Tricoli, A.; Pratsinis, S.E. *Chem. Mater.* **2010**, *22*, 3152−3157.
(11) Righettoni, M.; Tricoli, A.; Pratsinis, S. E. *Anal. Chem.* **2010**, *82*, 3581−3587.
(12) Shin, J. W.; Choi, S.-J.; Lee, I. K.; Youn, D.-Y.; Park, C. O.; Lee, J.-H.; Tuller, H. L.; Kim, I.-D. *Adv. Funct. Mater.* **2013**, *23*, 2357−2367.
(13) Spane, P.; Dryahina, K.; Smith, D. *J. Breath Res.* **2007**, *1*, 011001.
(14) Kim, H.-R.; Choi, K.-I.; Kim, K.-M.; Kim, I.-D.; Cao, G.; Lee, J.-H. *Chem. Commun.* **2011**, *10*, 5061−5063.
(15) Ratnawati.; Morton, J.; Henry, R. L.; Thomas, P. S. *Pediatr. Pulmonol.* **2006**, *41*, 929−936.
(16) Kuzmych, O.; Allen, B. L.; Star, A. *Nanotechnology* **2007**, *18*, 375502.
(17) Pijnenburg, M. W.; Hofhuis, W.; Hop, W. C.; De Jongste, J. C. *Thorax* **2005**, *60*, 215−218.
(18) Fruhberger, B.; Stirling, N.; Grillo, F. G.; Ma, S.; Ruthven, D.; Lad, R. J.; Frederick, B. G. *Sens. Actuators, B* **2001**, *76*, 226−234.
(19) Velasco-Arias, D.; Diaz, D.; Santiago-Jacinto, P.; Rodríguez-Gattorno, G.; Vazquez-Olmos, A.; Castillo-Blum, S. E. *J. Nanosci. Nanotechnol.* **2008**, *8*, 6389−6394.
(20) Barth, S.; Jimenez-Diaz, R.; Sama, J.; Prades, J. D.; I. Gracia, Santander, J.; Canec, C.; Romano-Rodriguez, A. *Chem. Commun.* **2012**, *48*, 4734−4736.
(21) Xiong, Y.; Mayers, B. T.; Xia, Y. *Chem. Commun.* **2005**, 5013−5022.
(22) Gao, T.; Wang, T. *Chem. Commun.* **2004**, 2558−2559.
(23) Rout, C. S.; Ganesh, K.; Govindaraj, A.; Rao, C. N. R. *Appl. Phys. A* **2006**, *85*, 241−246.
(24) Li, W.; Geng, X.; Guo, Y.; Rong, J.; Gong, Y.; Wu, L.; Zhang, X.; Li, P.; Xu, J.; Cheng, G.; Sun, M.; Liu, L. *ACS Nano* **2011**, *5*, 6955−6961.
(25) Choi, K. J.; Jang, H. W. *Sensors* **2010**, *10*, 4083−4099.
(26) Ahn, M.-W.; Park, K.-S.; Heo, J.-H.; Kim, D.-W.; Choi, K.J.; Park, J.-G. *Sens. Actuators, B* **2009**, *138*, 168−173.
(27) Liao, L.; Lu, H. B.; Shuai, M.; Li, J. C.; Liu, Y. L.; Liu, C.; Shen, Z. X.; Yu, T. *Nanotechnology* **2008**, *19*, 175501.
(28) Choi, Y.-J.; Hwang, I.-S.; Park, J.-G.; Choi, K. J.; Park, J.-H.; Lee, J.-H. *Nanotechnology* **2008**, *19*, 095508.
(29) Francioso, L.; Taurino, A. M.; Forleo, A.; Siciliano, P. *Sens. Actuators, B* **2008**, *130*, 70−76.
(30) Moon, H. G.; Shim, Y.-S.; Kim, D. H.; Jeong, H. Y.; Jeong, M. H.; Jung, J. Y.; Han, S. M.; Kim, J. K.; Kim, J.-S.; Park, H.-H.; Lee, J.-H.; Tuller, H. L.; Yoon, S.-J.; Jang, H. W. *Sci. Rep.* **2012**, *2*, 588.
(31) Hawkeye, M. M.; Brett, M. J. *J. Vac. Sci. Technol. A* **2007**, *25*, 1317−1335.
(32) Gouma, P. I.; Kalyanasundaram, K. *Appl. Phys. Lett.* **2008**, *93*, 244102.
(33) Kukkola, J.; Mohl, M.; Leino, A.-R.; Toth, G.; Wu, M.-C.; Shchukarev, A.; Popov, A.; Mikkola, J.-P.; Lauri, J.; Riihimaki, M.; Lappalainen, J.; Jantunen, H.; Kordas, K. *J. Mater. Chem.* **2012**, *22*, 17878−17886.
(34) Na, C. W.; Woo, H.-S.; Kim, I.-D.; Lee, J.-H. *Chem. Commun.* **2011**, *47*, 5148−5148.
(35) Bai, S. L.; Hu, J. W.; Li, D. Q.; Luo, R. X.; Chen, A. F.; Liu, C. C. *J. Mater. Chem.* **2011**, *21*, 12288−12294.
(36) Bai, S. L.; Chen, L. Y.; Yang, P. C.; Luo, R. X.; Chen, A. F.; Liu, C. C. *Sens. Actuators, B* **2008**, *135*, 1−6.
(37) You, L.; Sun, Y. F.; Ma, J.; Guan, Y.; J. Sun, M.; Du, Y.; Lu, G. Y. *Sens. Actuators, B* **2011**, *157*, 401−407.
(38) Teoh, L.G.; Hon, Y.M.; Shieh, J.; Lai, W. H.; Hon, M. H. *Sens. Actuators, B* **2003**, *96*, 219−225.
(39) Gill, M.; Walker, S.; Khan, A.; Green, S. M.; Kim, L.; Gray, S.; Krauss, B. *Acad. Emerg. Med.* **2005**, *12*, 579−586.
(40) Li, J.; Lu, Y. J.; Ye, Q.; Cinke, M.; Han, J.; Meyyappan, M. *Nano Lett.* **2003**, *3*, 929−933.
(41) Dua, V.; Surwade, S. P.; Ammu, S.; Agnihotra, S. R.; Jain, S.; Roberts, K. E.; Park, S.; Ruoff, R. S.; Manohar, S. K. *Angew. Chem., Int. Ed.* **2010**, *49*, 2154−2157.
(42) Xu, C.; Tamaki, J.; Miura, N.; Yamazoe, N. *Chem. Lett.* **1990**, *2*, 441−444.
(43) Xu, C.; Tamaki, J.; Miura, N.; Yamazoe, N. *Sens. Actuators, B* **1991**, *3*, 147−155.
(44) Yamazoe, N. *Sens. Actuators, B* **1991**, *5*, 7−19.
(45) Moon, H. G.; Shim, Y.-S.; Su, D.; Park, H.-H.; Yoon, S.-J.; Jang, H. W. *J. Phys. Chem. C* **2011**, *115*, 9993−9999.
(46) Lin, F.; Cheng, J.; Engtrakul, C.; Dillon, A. C.; Nordlund, D.; Moore, R. G.; Weng, T.-C.; Williams, S. K. R.; Richards, R. M. *J. Mater. Chem.* **2012**, *22*, 16817−16823.
(47) Qiu, Y.; Xu, G.-L.; Kuang, Q.; Sun, S.-G.; Yang, S. *Nano. Res.* **2012**, *5*, 826−832.
(48) Lee, J.; Mubeen, S.; Ji, X.; Stucky, G. D.; Moskovits, M. *Nano Lett.* **2012**, *12*, 5014−5019.
(49) Amano, F.; Li, D.; Ohtani, B. *Chem. Commun.* **2010**, *46*, 2769−2771.
(50) Yang, J.; Jiao, L.; Zhao, Q.; Wang, Q.; Gao, H.; Huan, Q.; Zheng, W.; Wang, Y.; Yuan, H. *J. Mater. Chem.* **2012**, *22*, 3699−3701.